

Pan-LUT: Efficient Pan-sharpening via Learnable Look-Up Tables

Zhongnan Cai^{1*} Yingying Wang^{1*} Yunlong Lin^{1*} Hui Zheng¹ Ge Meng¹
 ZiXu Lin¹ Jiaxin Xie¹ Junbin Lu² Yue Huang¹ Xinghao Ding^{1†}
¹Xiamen University
²University of Washington

Abstract

Recently, deep learning-based pan-sharpening algorithms have achieved notable advancements over traditional methods. However, many deep learning-based approaches incur substantial computational overhead during inference, especially with high-resolution images. This excessive computational demand limits the applicability of these methods in real-world scenarios, particularly in the absence of dedicated computing devices such as GPUs and TPUs. To address these challenges, we propose Pan-LUT, a novel learnable look-up table (LUT) framework for pan-sharpening that strikes a balance between performance and computational efficiency for high-resolution remote sensing images. To finely control the spectral transformation, we devise the PAN-guided look-up table (PG-LUT) for channel-wise spectral mapping. To effectively capture fine-grained spatial details and adaptively learn local contexts, we introduce the spatial details look-up table (SDLUT) and adaptive aggregation look-up table (AALUT). Our proposed method contains fewer than 300K parameters and processes a 8K resolution image in under 1 ms using a single NVIDIA GeForce RTX 2080 Ti GPU, demonstrating significantly faster performance compared to other methods. Experiments reveal that Pan-LUT efficiently processes large remote sensing images in a lightweight manner, bridging the gap to real-world applications. Furthermore, our model surpasses SOTA methods in full-resolution scenes under real-world conditions, highlighting its effectiveness and efficiency.

1. Introduction

High-resolution multispectral (HRMS) images are widely used in applications such as military operations, environmental monitoring, and mapping. However, due to the limitations of physical sensors, these images are challenging to obtain. Pan-sharpening addresses this issue by fus-

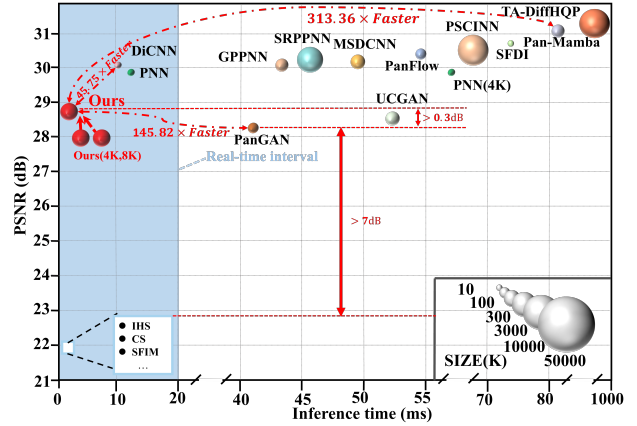


Figure 1. **Comparisons of performance and computational efficiency.** The PSNR value is evaluated on the Worldview-III dataset. Meanwhile, the inference time is measured on images with a resolution of (2048×2048) by employing a single NVIDIA GeForce RTX 2080 Ti GPU. Our method outperforms traditional approaches by a significant margin of 7 dB, while maintaining a speed comparable to that of traditional methods. Furthermore, our approach even surpasses some DNN-based approaches, outperforming Pan-GAN by more than 0.3 dB while being 145.82 times faster. Note that (4K, 8K) refer to models processing images at resolutions of 4096×4096 and 8192×8192 , respectively.

ing high-resolution panchromatic (PAN) images with low-resolution multispectral (LRMS) images, producing high-quality HRMS images through complementary integration [47] [55]. [61]. Recently, numerous pan-sharpening methods have been proposed, which can be generally categorized into two main groups: traditional methods and deep learning-based methods. Traditional pan-sharpening methods, such as component substitution (CS) [2] [3] [11], multi-resolution analysis (MRA) [7] [20], and variational optimization (VO) [10] [34], often struggle to restore precise spatial and spectral details in HRMS images. This limitation arises from their heavy reliance on manually designed features and insufficient modeling of prior knowledge. In contrast, deep learning-based pan-sharpening

* Equal contributions † Corresponding author.

methods have demonstrated exceptional fusion capabilities due to the powerful feature extraction ability of deep neural networks (DNNs). Masi et al. [32] built the Pan-sharpening Neural Network (PNN) model, which first applied CNN to pan-sharpening field, achieving a significant improvement over classical methods. Following this, researchers have explored more complicated and deeper networks to further promote the performance of pan-sharpening [12] [39] [33] [40] [56]. Besides, transformer-based models have garnered attention in pan-sharpening for their remarkable ability in long-range modeling, such as [53] [57] [59]. Nevertheless, many existing approaches suffer from significant computational overhead and memory costs during inference, particularly when dealing with high-resolution images. These excessive demands limit the practical deployment of these methods, especially in environments lacking dedicated computing resources such as GPUs and TPUs. As shown in Figure 1, very few methods are capable of processing 4K-resolution images under limited computational resources. Even among the deep learning-based methods that can handle 2K-resolution images, their inference speed is often suboptimal. In real-world applications, remote sensing images typically have much higher resolutions, and these methods may encounter significant challenges in operating efficiently under such conditions. Furthermore, simply increasing the depth of a network does not guarantee improved performance, as deeper networks become more difficult to train and may suffer from overfitting due to an excessive number of redundant parameters. To this end, our work aims to overcome these challenges by introducing a more efficient and lightweight pan-sharpening approach that delivers high performance and computational efficiency for high-resolution remote sensing images.

The lookup table (LUT), as a vital constituent in image signal processors (ISPs) [19], owes its significance to several advantageous characteristics, such as runtime efficiency and hardware-friendly nature. They offer a promising data structure for efficiently performing specific transformations by replacing expensive runtime computations with inexpensive array caching and indexing. However, the internal parameters of LUTs are usually preset by experts, making it difficult to optimize them for specific images, which limits their effectiveness.

To overcome the aforementioned challenges, we propose a novel learnable LUT framework, called Pan-LUT, which achieves a good balance between performance and computational efficiency in pan-sharpening. To finely control the spectral transformation, we devise the PAN-guided look-up table (PGLUT) for channel-wise spectral mapping. To effectively capture fine-grained spatial details and adaptively learn local contexts, we introduce the spatial details look-up table (SDLUT) and adaptive aggregation look-up table (AALUT). Our method consists of fewer than 300K param-

eters and can process a 8K resolution image in under 1 ms using a single NVIDIA GeForce RTX 2080 Ti GPU. Furthermore, our approach outperforms traditional methods by 7 dB, while maintaining a speed comparable to that of conventional techniques, demonstrating superior speed and efficiency compared to existing methods.

In summary, the contributions are as follows:

- We present Pan-LUT, a novel learnable LUT framework that does not incorporate any network structure. This framework is designed to achieve a strong balance between performance and computational efficiency in pan-sharpening high-resolution remote sensing images.
- To finely control the spectral transformation, we devise the PAN-guided look-up table (PGLUT) for channel-wise spectral mapping. To effectively capture fine-grained spatial details and adaptively learn local contexts, we introduce the spatial details look-up table (SDLUT) and adaptive aggregation look-up table (AALUT).
- To the best of our knowledge, this is the first attempt to introduce LUTs for efficient pan-sharpening. Extensive experiments on different satellite datasets demonstrate the effectiveness and efficiency of Pan-LUT.

2. Related Works

2.1. Look-Up Table

Lookup Table (LUT) is a widely-used data structure in Image Signal Processors (ISPs) [5] [8] [18], which maps a set of indices to corresponding output values, allowing efficient retrieval without the need for repeated computations. LUTs are particularly useful for functions of multiple variables, as they store precomputed outputs for all possible input combinations. For example, in a 1D LUT, a single input index is mapped to an output value, often using linear interpolation for indices that fall between pre-stored values. More complex LUTs, such as 3D LUTs, use three independent input variables, which may require advanced interpolation methods like trilinear or tetrahedral interpolation. Due to its portability, various LUT based solutions have been proposed for image enhancement [6] [23] [26, 27]. For instance, Zeng et al. [52] and Wang et al. [38] propose image-adaptive 3D LUTs for efficient single-image enhancement. These approaches rely on a network weight predictor to fuse different 3D LUTs, which may pose a limitation on platforms under resource-constrained conditions. Additionally, LUT-based methods have been explored in the area of super-resolution [17] [22] [30] [28]. SRLUT [17] trains a deep super-resolution (SR) network with a restricted receptive field and then cache the output values from the learned SR network in LUTs. However, issues such as performance degradation arise when large patches are cached in LUTs, prompting the development of strategies like MuLUT [22], which introduces multiple LUT variants and a fine-tuning strategy to improve performance. To further enhance the

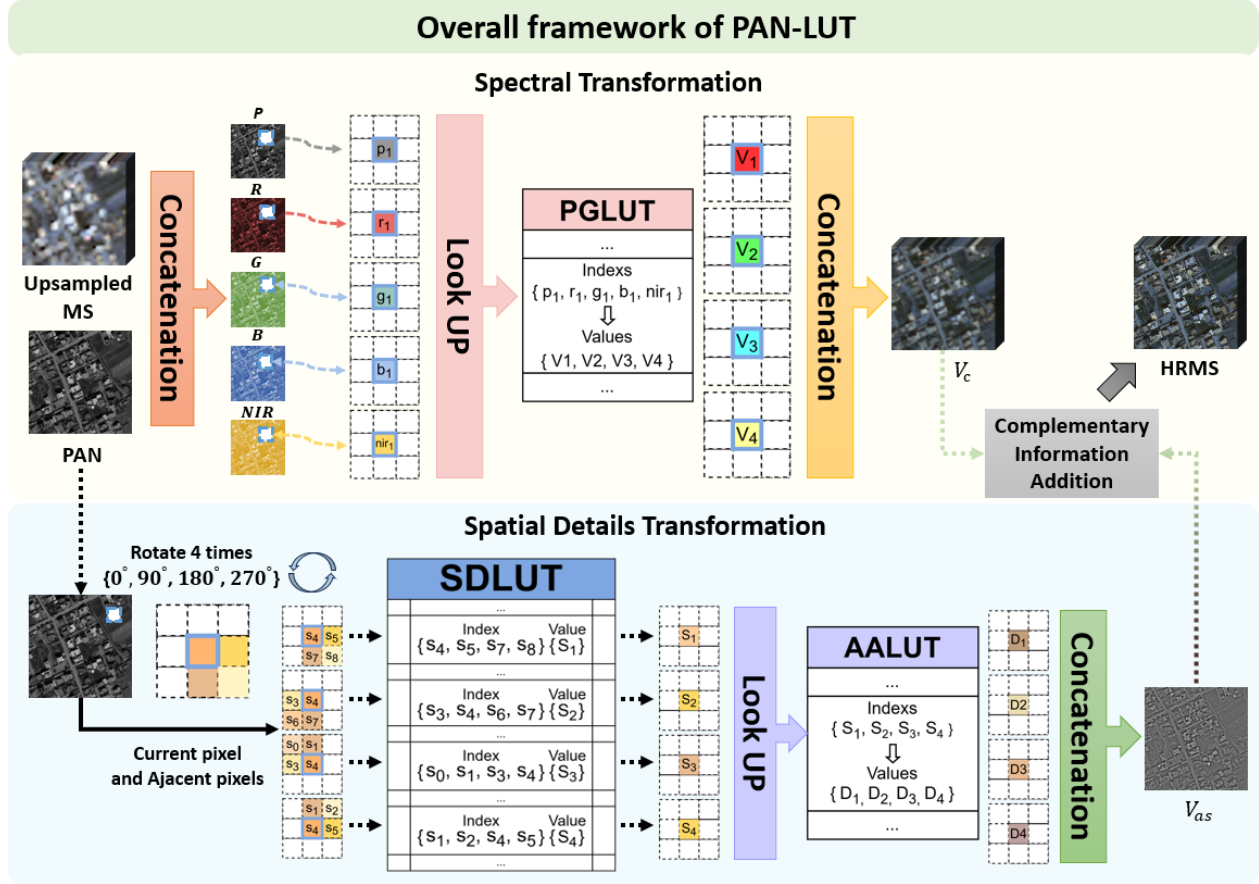


Figure 2. **The overall framework of our proposed Pan-LUT.** To finely control the spectral transformation, we devise the PAN-guided look-up table (PGLUT) for channel-wise spectral mapping. To effectively capture fine-grained spatial details and adaptively learn local contexts, we introduce the spatial details look-up table (SDLUT) and adaptive aggregation look-up table (AALUT).

functionality of LUTs, architectures like SPLUT [30] and RCLUT [28] have been proposed. SPLUT processes different image information separately using multiple LUTs, while RCLUT introduces a plugin module to improve LUT-based models with minimal additional computational cost.

2.2. Traditional Pan-sharpening Methods

Traditional fusion techniques encompass component substitution (CS), multi-resolution analysis (MRA), and variational optimization (VO). CS methods, such as IHS [2], Brovey [11], and PCA [3], utilize spatial details from high-resolution panchromatic (PAN) images to replace corresponding details in low-resolution multispectral (LRMS) images, often causing spectral distortion due to the incomplete incorporation of spectral information. MRA techniques, including DWT [20] and ATWT [7], apply multi-resolution decomposition to merge PAN and LRMS images, which helps to reduce spectral distortion. VO methods, such as Bayesian [10] and Total Variation [34], formulate the fusion process as an optimization problem by iteratively minimizing the loss function. While VO methods show promis-

ing results, they encounter challenges in optimizing model design and loss functions. Although these approaches have yielded certain improvements, their performance remains constrained by the inadequate modeling, which restricts further advancements in pan-sharpening accuracy and quality.

2.3. Deep Learning-based Methods

Deep learning-based methods have emerged as the dominant approach for pan-sharpening in recent years. The PNN [32] model, inspired by SRCNN [9], is the first to introduce CNNs into this domain, surpassing traditional methods. Models like PanNet [49] and MSDCNN [50] further enhance performance by leveraging residual connections and multi-scale convolutions, effectively capturing high-frequency details and supporting a wide range of remote sensing applications. Since then, more complex CNN-based architectures [4] [14] [15] [62] [41] have been proposed in this field to improve pan-sharpening's mapping ability. Models like GPPNN [44], MMNet [46], and ARFNet [45], which enhance interpretability through deep unfolding techniques and accelerate model conver-

Table 1. Quantitative comparison across three satellite datasets. The best outcomes are highlighted in red. \uparrow indicates better performance with increasing values, while \downarrow signifies improved performance with decreasing values.

Method	WorldView-II				GaoFen2				Worldview-III				Inference (ms)		
	PSNR \uparrow	SSIM \uparrow	SAM \downarrow	ERGAS \downarrow	PSNR \uparrow	SSIM \uparrow	SAM \downarrow	ERGAS \downarrow	PSNR \uparrow	SSIM \uparrow	SAM \downarrow	ERGAS \downarrow	1024 \times 1024	2048 \times 2048	4096 \times 4096
Brovey [11]	35.8646	0.9216	0.0403	1.8238	37.7974	0.9026	0.0218	1.3720	22.5060	0.5466	0.1159	8.2331	0.20	0.21	0.23
IHS [2]	35.2962	0.9027	0.0461	2.0278	38.1754	0.9100	0.0243	1.5336	22.5579	0.5354	0.1266	8.3616	0.20	0.21	0.23
SFIM [29]	34.1297	0.8975	0.0439	2.3449	36.9060	0.8882	0.0318	1.7398	21.8212	0.5457	0.1208	8.9730	0.26	0.29	0.33
GS [21]	35.6376	0.9176	0.0423	1.8774	37.2260	0.9034	0.0309	1.6736	22.5608	0.5470	0.1217	8.2433	0.68	0.73	0.76
PNN [32]	40.7550	0.9624	0.0259	1.0646	43.1208	0.9704	0.0172	0.8528	29.9418	0.9121	0.0824	3.3206	4.21	12.81	54.59
MSDCNN [50]	41.3355	0.9664	0.0242	0.9940	45.6847	0.9827	0.0135	0.6389	30.3038	0.9184	0.0782	3.1884	16.45	49.82	OOM
Pan-GAN [31]	39.1025	0.9562	0.0303	1.2954	41.4468	0.9661	0.0205	1.0593	28.4959	0.8897	0.0998	3.9067	14.55	40.83	OOM
GPPNN [44]	41.1622	0.9684	0.0244	1.0315	44.2145	0.9815	0.0137	0.7361	30.1785	0.9175	0.0776	3.2593	17.59	43.60	OOM
SFDI [60]	41.7244	0.9725	0.0220	0.9506	47.4712	0.9901	0.0102	0.5462	30.5971	0.9236	0.0741	3.0798	20.26	65.37	OOM
UCGAN [58]	40.0545	0.9553	0.0275	1.1734	42.3634	0.9557	0.0194	0.9480	28.6705	0.8851	0.0990	3.8696	17.26	52.06	OOM
PanFlow [48]	41.8584	0.9712	0.0224	0.9335	47.2533	0.9884	0.0103	0.5512	30.4873	0.9221	0.0751	3.1142	18.27	54.19	OOM
PSCINN [37]	41.8520	0.9703	0.0223	0.9407	47.1100	0.9878	0.0107	0.5612	30.5599	0.9230	0.0748	3.1033	28.31	60.74	OOM
Pan-Mamba [13]	42.2354	0.9729	0.0212	0.8975	47.6453	0.9894	0.0103	0.5286	31.1551	0.9299	0.0702	2.8942	42.31	87.74	OOM
TA-DiffHQP [41]	42.1255	0.9752	0.0211	0.9023	47.7716	0.9900	0.0101	0.5378	31.3369	0.9302	0.0737	2.6369	481.27	998.58	OOM
Pan-LUT (Ours)	39.8362	0.9555	0.0286	1.1695	42.6559	0.9642	0.0189	0.9044	28.8213	0.8936	0.0935	3.7520	0.27	0.28	0.30

gence. Other approaches, including SFDI [60] and MS-DDN [50], utilize Fourier transforms to capture high-frequency features. Transformer-based architectures, such as INN-former [59], Panformer [57] and DRFormer [53] combine CNNs and Transformers to capture both local and global features. Instead of learning a deterministic mapping, generative models such as UCGAN [58], PanFlow [48] and PSCINN [37] generate a distribution of possible outputs for the given inputs. Additionally, some networks [25] [54] [42] [24] focus on improving the generalization capability of CNN-based fusion models by learning generalized features. Despite their promising results, these advanced methods come with high computational costs, limiting their practical applicability.

3. Method

Given the PAN image ($P \in R^{H \times W \times 1}$) and the MS image ($MS \in R^{H/r \times W/r \times C}$), pan-sharpening aims to fuse the complementary information to generate the desirable high spatial resolution MS image ($HRMS \in R^{H \times W \times C}$). Here, H and W denote the height and width of the images, r represents the spatial resolution ratio, with a value of 4, and C denotes the number of spectral bands.

3.1. Framework

The overall framework of our proposed Pan-LUT is illustrated in Figure 2. To finely control the spectral transformation, we devise the PAN-guided look-up table (PGLUT) for channel-wise spectral mapping. To effectively capture fine-grained spatial details and adaptively learn local contexts, we introduce the spatial details look-up table (SDLUT) and adaptive aggregation look-up table (AALUT). Specifically, given the PAN image ($P \in R^{H \times W \times 1}$) and the upsampled

MS image ($MS \in R^{H \times W \times C}$), they are first concatenated to form $PM \in R^{H \times W \times (C+1)}$, which is then fed into PGLUT for channel-wise spectral mapping, producing the output $V_c \in R^{H \times W \times C}$. SDLUT, using only the PAN image as input, generates local spatial details $V_s \in R^{H \times W \times C}$. To further enhance spatial representation, AALUT takes $V_s \in R^{H \times W \times C}$ as input to adaptively learn local contexts, resulting in $V_{as} \in R^{H \times W \times C}$. By summing up V_c and V_{as} , we can obtain the final HRMS result:

$$\begin{aligned}
 V_c &= PGLUT(PM), \\
 V_s &= SDLUT(P), V_{as} = AALUT(V_s), \\
 HRMS &= V_c + V_{as}.
 \end{aligned} \tag{1}$$

3.2. Spectral Transformation

To preserve the rich spectral information of the MS image, we propose the PAN-guided look-up table (PGLUT), which leverages the PAN image as guidance to finely control the spectral transformation. Specifically, PGLUT is represented as a 5-dimensional matrix containing N^5 elements, where N denotes the number of bins in each dimension. Each element corresponds to a sampling point, defining a set of indexed input pixels $\{I_{(i,j,k,m,n)}\}_{i,j,k,m,n=0,\dots,N-1}$ and their corresponding output pixels $\{O_{(i,j,k,m,n)}\}_{i,j,k,m,n=0,\dots,N-1}$. Here, $I \in \{pa, r, g, b, nir\}$ represents the pixel values from the PAN and MS images, while $O \in \{R, G, B, NIR\}$ denotes the corresponding cached output pixels.

Since the distribution of LUT elements is discrete in space, the output value cannot be directly retrieved from the LUT. For an input value $\{pa_{(w,h)}^I, r_{(w,h)}^I, g_{(w,h)}^I, b_{(w,h)}^I, nir_{(w,h)}^I\}$, where (w, h) denotes the spatial position of a pixel in the image.

PGLUT first performs a lookup operation to locate the corresponding input pixel in the LUT:

$$\begin{aligned} x &= \frac{pa_{(w,h)}^I}{V_{max}} \cdot N, y = \frac{r_{(w,h)}^I}{V_{max}} \cdot N, z = \frac{g_{(w,h)}^I}{V_{max}} \cdot N, \\ s &= \frac{b_{(w,h)}^I}{V_{max}} \cdot N, e = \frac{nr_{(w,h)}^I}{V_{max}} \cdot N, \end{aligned} \quad (2)$$

where V_{max} denotes the maximum value (e.g., 255, 1023 or 2047). The coordinates of the sampling points, $L = \{(i+c, j+c, k+c, m+c, n+c)\}$, with $c \in \{0, 1\}$, can be derived as follows:

$$i = \lfloor x \rfloor, j = \lfloor y \rfloor, k = \lfloor z \rfloor, m = \lfloor s \rfloor, n = \lfloor e \rfloor, \quad (3)$$

where $\lfloor \cdot \rfloor$ denotes the floor function. $\{\mathbf{d}_l\}_{l=x,y,z,s,e}$ represents the offset of the input index (x, y, z, s, e) relative to the defined sampling point (i, j, k, m, n) , e.g., $\mathbf{d}_x = x - i$.

After locating 32 adjacent points, an appropriate interpolation technique is applied to generate the output value using the values of these sampled points:

$$O_{(x,y,z,s,e)} = PInterpolation(LUT[L], \{\mathbf{d}_l\}), \quad (4)$$

where $PInterpolation(\cdot)$ denotes the pentilinear interpolation.

3.3. Spatial Details Transformation

PGLUT is essentially a channel-wise 5D LUT that operates globally, which limits its ability to capture local spatial information. To effectively capture fine-grained spatial details and adaptively learn local contexts, we propose the Spatial Details Lookup Table (SDLUT) and the Adaptive Aggregation Lookup Table (AALUT). As illustrated in Figure 2, given a pixel $p_{(w,h)}$, SDLUT processes this pixel along with its neighboring pixels as input. During the training phase, we employ a rotation ensemble strategy to further expand the receptive field, which can be formulated as:

$$\begin{aligned} V_1 &= f(p_{(w,h)}, p_{(w+1,h)}, p_{(w,h+1)}, p_{(w+1,h+1)}), \\ V_2 &= f(p_{(w,h)}, p_{(w+1,h)}, p_{(w+1,h-1)}, p_{(w,h-1)}), \\ V_3 &= f(p_{(w,h)}, p_{(w+1,h)}, p_{(w,h+1)}, p_{(w+1,h+1)}), \\ V_4 &= f(p_{(w,h)}, p_{(w+1,h)}, p_{(w,h+1)}, p_{(w+1,h+1)}). \end{aligned} \quad (5)$$

Subsequently, a learnable AALUT is introduced to adaptively integrates the four outputs. Specially, the AALUT takes the output from SDLUT as input and combines the spatial information to enhance the spatial representation:

$$V_{as} = f_{AALUT}(V_1, V_2, V_3, V_4), \quad (6)$$

where $f_{AVGLUT}(\cdot)$ denotes the lookup and interpolation process in the LUT retrieval.

3.4. Loss Function

To achieve satisfying pan-sharpening results, we propose a joint loss for network training. We first utilize the L1 loss:

$$\mathcal{L}_1 = \|HRMS - GT\|_1, \quad (7)$$

where $HRMS$ and GT denote the network output and the corresponding ground truth, respectively.

To enhance the stability and robustness of the learned LUTs, we incorporate smoothness regularization \mathcal{L}_s and monotonicity regularization \mathcal{L}_m :

$$\mathcal{L}_s = \mathcal{L}_s^{PG} + \mathcal{L}_s^{SD} + \mathcal{L}_s^{AA}, \quad (8)$$

$$\mathcal{L}_m = \mathcal{L}_m^{PG} + \mathcal{L}_m^{SD} + \mathcal{L}_m^{AA}, \quad (9)$$

where \mathcal{L}_s^{PG} , \mathcal{L}_s^{SD} , and \mathcal{L}_s^{AA} denote the smoothness regularizations for PGLUT, SDLUT, and AALUT, while \mathcal{L}_m^{PG} , \mathcal{L}_m^{SD} , and \mathcal{L}_m^{AA} represent the monotonicity regularizations for PGLUT, SDLUT, and AALUT, respectively.

Taking AALUT as an example, the smoothness regularization can be defined as:

$$\begin{aligned} \mathcal{L}_s^{AA} &= \sum_{O \in \{l,o,c,a\}} \sum_{i,j,k,m=0}^{N-1} (\|O_{(i+1,j,k,m)} - O_{(i,j,k,m)}\|^2 \\ &\quad + \|O_{(i,j+1,k,m)} - O_{(i,j,k,m)}\|^2 \\ &\quad + \|O_{(i,j,k+1,m)} - O_{(i,j,k,m)}\|^2 \\ &\quad + \|O_{(i,j,k,m+1)} - O_{(i,j,k,m)}\|^2), \end{aligned} \quad (10)$$

where N represents the number of bins in each dimension of the LUT. $O_{(i,j,k,m)}$ is the corresponding output for the defined sampling point (i, j, k, m) in LUT. The definitions of \mathcal{L}_s^{PG} and \mathcal{L}_s^{SD} are similar to those in Eq. (10).

The monotonicity regularization in AALUT can be defined as:

$$\begin{aligned} \mathcal{L}_m^{AA} &= \sum_{O \in \{l,o,c,a\}} \sum_{i,j,k,m=0}^{N-1} [g(O_{(i,j,k,m)} - O_{(i+1,j,k,m)}) \\ &\quad + g(O_{(i,j,k,m)} - O_{(i,j+1,k,m)}) \\ &\quad + g(O_{(i,j,k,m)} - O_{(i,j,k+1,m)}) \\ &\quad + g(O_{(i,j,k,m)} - O_{(i,j,k,m+1)})], \end{aligned} \quad (11)$$

where $g(\cdot)$ denotes the ReLU activation function. Similarly, \mathcal{L}_m^{PG} and \mathcal{L}_m^{SD} are defined in the same way as in Eq. (11).

The final loss functions are as follows:

$$\mathcal{L} = \mathcal{L}_1 + \lambda_s \mathcal{L}_s + \lambda_m \mathcal{L}_m, \quad (12)$$

where the two constant parameters λ_s and λ_m are used to control the effects of the smoothness and monotonicity regularization terms, respectively. In our experiments, we empirically set $\lambda_s = 0.0001$ and $\lambda_m = 10$.

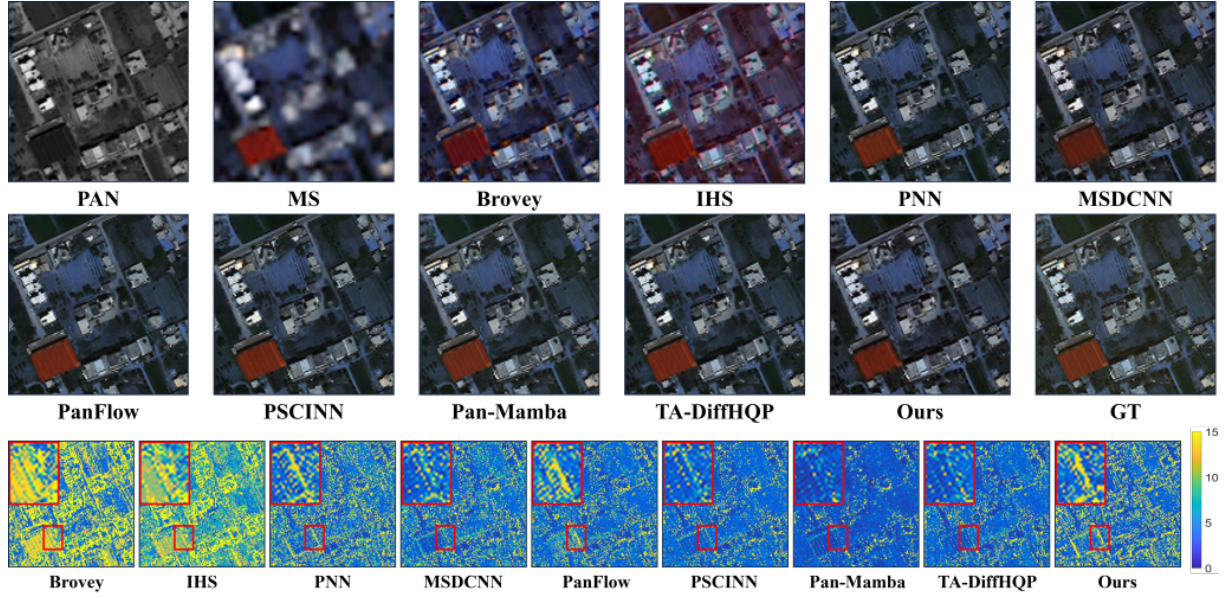


Figure 3. Visual comparison on WorldView-III dataset. The last row visualizes the MSE residues between the pan-sharpening results and the ground truth.

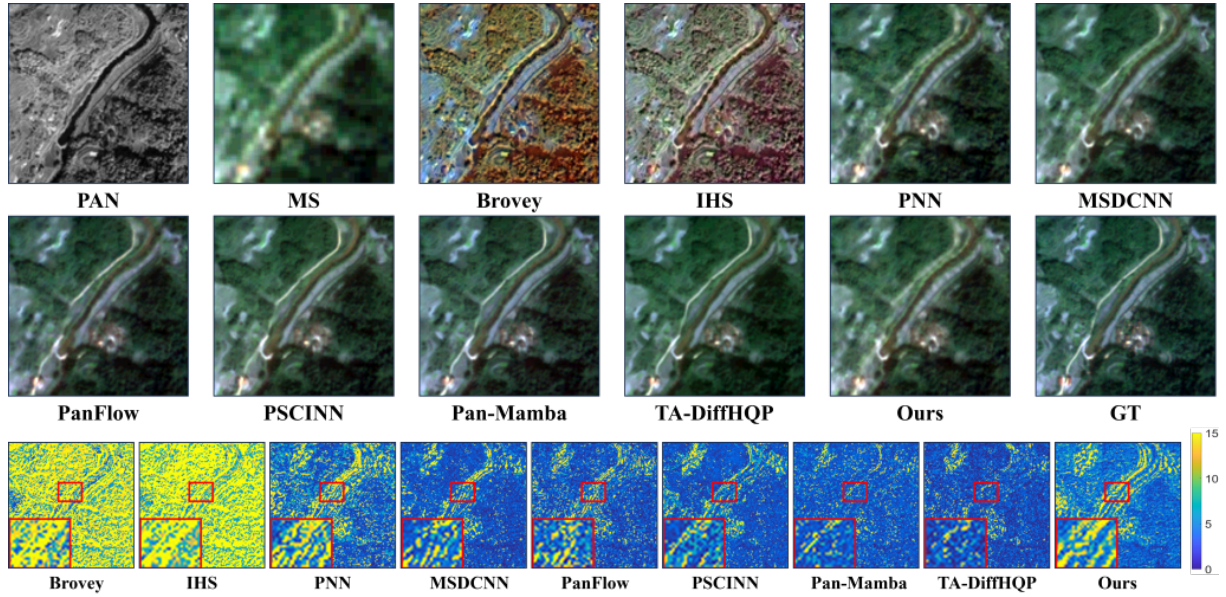


Figure 4. Visual comparison on GaoFen2 dataset. The last row visualizes the MSE residues between the pan-sharpening results and the ground truth.

4. Experiments

In this section, we provide a comprehensive overview of the experimental setup, including the evaluation datasets, performance metrics, and implementation details. We then present both quantitative and qualitative comparisons with other methods. Additionally, we conduct ablation studies to validate the contribution of each component.

4.1. Datasets

Remote sensing datasets from three satellites are used in our experiments, including WorldView-II (WV2), GaoFen2

(GF2) and WorldView-III (WV3). Due to the absence of high-resolution multispectral ground truth images in these datasets, we generate the training set using the Wald protocol tool [36]. Specifically, given the original MS image and its corresponding high-resolution PAN image, they are downsampled by a factor of r to obtain image pairs of MS and PAN, with r set to 4. During training, the original high-resolution MS image is treated as the ground truth, while the MS and PAN images serve as the input image pairs.

Table 2. Evaluation on the real-world full-resolution scenes from WorldView-II dataset. The best values are highlighted by red. The up or down arrow indicates higher or lower metric corresponding to better results.

Metrics	Brovey	IHS	PNN	MSDCNN	GPPNN	SFDI	UCGAN	PanFlow	PSCINN	Pan-Mamba	TA-DiffHQP	Ours
$D_\lambda \downarrow$	0.1026	0.1110	0.1057	0.1063	0.0987	0.1034	0.1042	0.0966	0.0967	0.0966	0.0953	0.0962
$D_S \downarrow$	0.1409	0.1556	0.1446	0.1443	0.1312	0.1305	0.1476	0.1274	0.1271	0.1272	0.1129	0.1253
QNR \uparrow	0.7728	0.7527	0.7684	0.7683	0.7859	0.7827	0.7650	0.7910	0.7904	0.7911	0.8025	0.7985

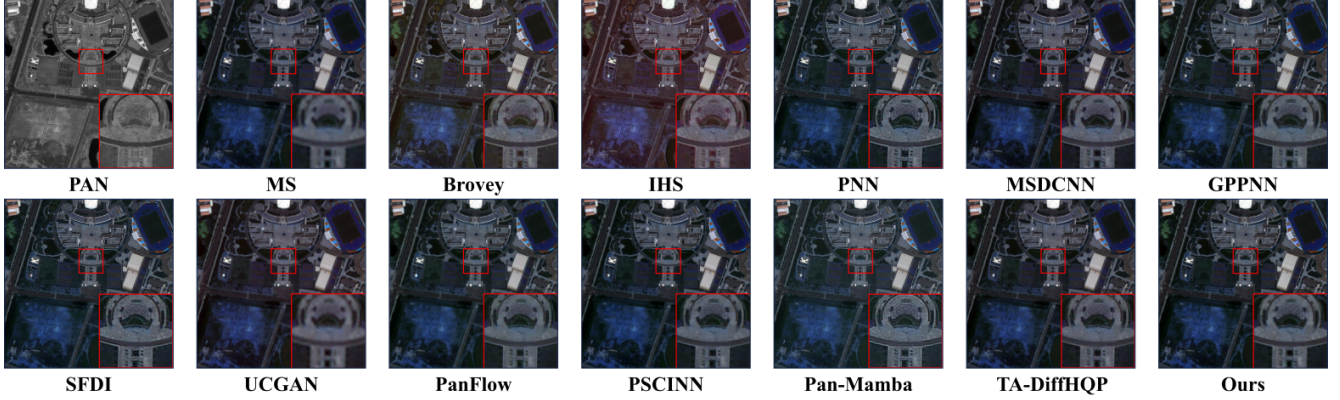


Figure 5. Visual comparison on the real full-resolution scenes from the WorldView-II dataset. For a more detailed examination of the results, we zoomed-in view on specific parts of the images.

4.2. Implementation Details

We compare the proposed Pan-LUT against several pan-sharpening methods on reduced-resolution scenes from WV2, WV3, and GF2 datasets. Specifically, we choose four traditional pan-sharpening techniques: Brovey [11], IHS [2], SFIM [29] and GS [21], along with ten deep learning-based approaches: PNN [32], MSDCNN [50], Pan-GAN [31], SFDI [60], UCGAN [58], PanFlow [48], PSCINN [37], Pan-Mamba [13] and TA-DiffHQP [41].

Several widely used image quality assessment metrics are employed to evaluate the performance of the algorithm, including peak signal-to-noise ratio (PSNR) [16], structural similarity index (SSIM) [43], spectral angle mapper (SAM) [51], relative dimensionless global error in synthesis (ERGAS) [35], spectral distortion index (D_λ), spatial distortion index (D_S) and the quality with no reference (QNR) [1]. As our goal is to perform pan-sharpening under resource-constrained conditions for high-resolution remote sensing images, we then conduct the experiments on a single NVIDIA GeForce RTX 2080Ti GPU, using full-resolution scenes under real-world conditions. The PyTorch framework is implemented in our experiment. During the training phase, we employ an ADAM optimizer with $\beta_1 = 0.9$ and $\beta_2 = 0.999$, to update the network parameters for 600 epochs with a batch size of 1. The learning rate is initialized with 3×10^{-4} . In parallel, a StepLR learning rate adjustment strategy is employed to reduce the learning rate by half after every 200 iterations. The sizes of PGLUT, SDLUT and AALUT are set to 9, 9 and 9, respectively.

4.3. Comparison with Other Methods

Evaluation on Reduced-resolution Scene. The quantitative results across three datasets are presented in Table 1, with the best results highlighted in red. Compared to traditional methods, our approach achieves an average PSNR improvement of 4dB, 5dB, and 6dB across the three datasets, while maintaining inference speeds comparable to those of traditional methods. Compared to DNN-based methods, our method exhibits an average PSNR performance decrease of 2 dB, 4 dB, and 2 dB across the three datasets. However, as shown in the table, only PNN is capable of processing 4K-resolution images. Notably, our method is 181.97 times faster than PNN, while the performance gap remains minimal at 0.92 dB, 0.46 dB, and 1.12 dB across the three datasets. It is worth noting that the proposed Pan-LUT does not incorporate any network structure, yet it outperforms some DNN-based methods, such as Pan-GAN and UCGAN, in terms of both performance and inference time. We also provide visual comparisons for the WorldView-III and GaoFen2 datasets, as shown in Figure 3 and Figure 4. **Evaluation on Full-resolution Scene.** To assess the performance and generalization capability of our method on full-resolution scenes under real-world conditions, we first trained Pan-LUT on WorldView-II data and then tested it on unseen full-resolution WorldView-II satellite datasets. The real-world dataset consists of 200 newly collected samples from the WorldView-II satellite for evaluation. The results are presented in Table 2. On reduced-resolution scenes, our method falls short of most DNN-based approaches in terms of performance. How-

ever, on full-resolution scenes, it outperforms the majority of them when considering the metrics of D_λ , D_S , and QNR. This demonstrates its strong generalization ability in real-world situations. Additionally, we provide a visual comparison against both traditional and DNN-based methods, as shown in Figure 5. **Evaluation on Reduced-resolution Scene.** There are two key limitations of DNN-based methods in practical applications. First, real-world remote sensing satellite images typically possess extremely large sizes, thereby incurring substantial computational burdens. Second, computational resources are often limited, which further restricts the applicability of these methods. Therefore, we conduct comparative experiments to evaluate the computational efficiency of various methods on high-resolution images, including 1024×1024 , 2048×2048 and 4096×4096 resolutions. For each method, we record the average inference time on 100 images, with all inference steps conducted on a single NVIDIA GeForce RTX 2080Ti GPU for fair comparison. As shown in Table 1, Pan-LUT efficiently processes images at all resolutions. Compared to DNN-based methods, it achieves significantly faster inference speeds, while maintaining comparable speed to traditional methods. Our method easily meets the real-time processing requirements on GPUs, outperforming all other methods by a substantial margin. Notably, only PNN is capable of handling remote sensing satellite images at the 4096×4096 resolution, highlighting the superior efficiency of our approach.

5. Ablation Study

In this section, we conduct several ablation studies on the WorldView-III dataset to investigate the impact of LUT size and evaluate the effectiveness of each proposed component. **Size of Look-Up Tables.** As shown in Figure 6, changing the LUT size does not lead to a significant drop in performance. This observation suggests that the effectiveness of our proposed method is not dependent on consuming extensive storage resources to increase the LUT size.

First, we explore the effect of PGLUT size, denoted N_P . Performance improves with larger N_P , reaching an optimal point at values $N_P = 9$. Beyond this (from 9 to 17), only a small gain of 0.005 dB is observed, while the parameters increase substantially from 236K to 5M, indicating capacity redundancy. We therefore set $N_P = 9$ as the default to balance performance with storage requirements.

For SDLUT, denoted N_S , we find that increasing N_S from 3 to 9 improves performance, but values above 9 cause a slight performance drop.

Similarly, enlarging AALUT size N_A yields only minor gains but substantially increases parameters, especially beyond $N_A = 9$. We set $N_A = 9$ to balance performance with computational efficiency. **Effectiveness of Each LUT.** We further conduct ablation studies to verify the effectiveness

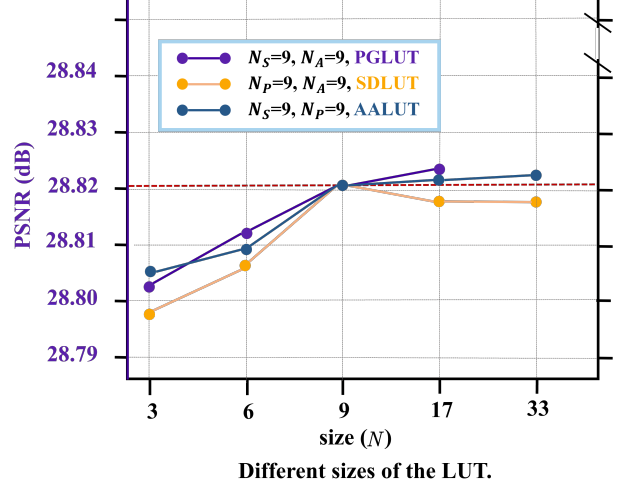


Figure 6. Ablation studies on different sizes of the PGLUT, SDLUT and AALUT on the WorldView-III dataset.

Table 3. Ablation study of PGLUT, SDLUT and AALUT on the WorldView-III dataset.

Config	PSNR↑	SSIM↑	SAM↓	ERGAS↓
(i)	23.2254	0.5602	0.1071	7.5064
(ii)	25.9433	0.8132	0.1495	5.5512
(iii)	28.1315	0.8695	0.1183	4.1885
(iv)	26.5035	0.8297	0.1251	5.1258
★ Pan-LUT (Ours)	28.8213	0.8936	0.0935	3.7520

of each LUT. Specifically, we examine the following four settings: (i) only PGLUT, (ii) only SDLUT, (iii) PGLUT and SDLUT, and (iv) SDLUT and AALUT. For (i), the output of PGLUT is directly used as the result. For (ii), the outputs of SDLUT are averaged and then added to the MS image. For (iii), the averaged SDLUT outputs are added to the PGLUT output to generate the result. For (iv), AALUT takes the output of SDLUT as input and performs adaptive aggregation to produce the final result. Results are listed in Table 3. Our observations are as follows: 1) Comparing (i) and (iii), SDLUT effectively captures fine-grained spatial details from the PAN image, thereby enhancing overall performance. 2) Comparing (ii) and (iii), PGLUT provides finer control over spectral transformation, resulting in improved performance. 3) Comparing (ii) and (iv), AALUT demonstrates adaptive aggregation capabilities, effectively learning local contexts and clearly outperforming simple averaging.

6. Conclusion

In this paper, we propose a novel learnable LUT framework, called Pan-LUT, which strikes an optimal balance between performance and computational efficiency for high-resolution remote sensing images in pan-sharpening. To

effectively handle high-resolution images under resource-constrained conditions, we design PGLUT to finely control spectral transformations and facilitate channel-wise spectral mapping. Additionally, we introduce SDLUT and AALUT to capture fine-grained spatial details and adaptively learn local contexts. Extensive experiments on various satellite datasets demonstrate the effectiveness and efficiency of Pan-LUT.

References

- [1] Luciano Alparone, Bruno Aiazzi, Stefano Baronti, Andrea Garzelli, Filippo Nencini, and Massimo Selva. Multispectral and panchromatic data fusion assessment without reference. *Photogrammetric Engineering & Remote Sensing*, 74(2):193–200, 2008. 7
- [2] Wjoseph Carper, Thomasm Lillesand, Ralphw Kiefer, et al. The use of intensity-hue-saturation transformations for merging spot panchromatic and multispectral image data. *Photogrammetric Engineering and remote sensing*, 56(4):459–467, 1990. 1, 3, 4, 7
- [3] PatS. Chavez and AndyY. Kwarteng. Extracting spectral contrast in landsat thematic mapper image data using selective principal component analysis. *Photogrammetric Engineering and Remote Sensing*, 1989. 1, 3
- [4] Yingxia Chen, Huiqi Liu, and Faming Fang. A novel pansharpening method based on cross stage partial network and transformer. *Scientific reports*, 14(1): 12631, 2024. 3
- [5] Marcos V Conde, Steven McDonagh, Matteo Maggioni, Ales Leonardis, and Eduardo Pérez-Pellitero. Model-based image signal processors via learnable dictionaries. In *Proceedings of the AAAI Conference on Artificial Intelligence*, pages 481–489, 2022. 2
- [6] Marcos V Conde, Javier Vazquez-Corral, Michael S Brown, and Radu Timofte. Nilut: Conditional neural implicit 3d lookup tables for image enhancement. In *Proceedings of the AAAI Conference on Artificial Intelligence*, pages 1371–1379, 2024. 2
- [7] Farzaneh DadrasJavan, Farhad Samadzadegan, and Fatemeh Fathollahi. Spectral and spatial quality assessment of ihs and wavelet based pan-sharpening techniques for high resolution satellite imagery. *Image Video Process*, 6(1), 2018. 1, 3
- [8] Mauricio Delbracio, Damien Kelly, Michael S Brown, and Peyman Milanfar. Mobile computational photography: A tour. *Annual review of vision science*, 7(1): 571–604, 2021. 2
- [9] Chao Dong, Chen Change Loy, Kaiming He, and Xiaoou Tang. Image super-resolution using deep convolutional networks. *IEEE transactions on pattern analysis and machine intelligence*, 38(2):295–307, 2015. 3
- [10] Dominique Fasbender, Julien Radoux, and Patrick Boagaert. Bayesian data fusion for adaptable image pansharpening. *IEEE Transactions on Geoscience and Remote Sensing*, 46(6):1847–1857, 2008. 1, 3
- [11] Alan R Gillespie, Anne B Kahle, and Richard E Walker. Color enhancement of highly correlated images. ii. channel ratio and “chromaticity” transformation techniques. *Remote Sensing of Environment*, page 343–365, 1987. 1, 3, 4, 7
- [12] Xuanhua He, Keyu Yan, Rui Li, Chengjun Xie, Jie Zhang, and Man Zhou. Pyramid dual domain injection network for pan-sharpening. In *Proceedings of the IEEE/CVF International Conference on Computer Vision (ICCV)*, pages 12908–12917, 2023. 2
- [13] Xuanhua He, Ke Cao, Jie Zhang, Keyu Yan, Yingying Wang, Rui Li, Chengjun Xie, Danfeng Hong, and Man Zhou. Pan-mamba: Effective pan-sharpening with state space model. *Information Fusion*, 115:102779, 2025. 4, 7
- [14] Junming Hou, Qi Cao, Ran Ran, Che Liu, Junling Li, and Liang-jian Deng. Bidomain modeling paradigm for pansharpening. In *Proceedings of the 31st ACM International Conference on Multimedia*, pages 347–357, 2023. 3
- [15] Jingjia Huang, Ge Meng, Yingying Wang, Yunlong Lin, Yue Huang, and Xinghao Ding. Dp-innet: Dual-path implicit neural network for spatial and spectral features fusion in pan-sharpening. In *Chinese Conference on Pattern Recognition and Computer Vision (PRCV)*, pages 268–279. Springer, 2023. 3
- [16] Quan Huynh-Thu and Mohammed Ghanbari. Scope of validity of psnr in image/video quality assessment. *Electronics letters*, 44(13):800–801, 2008. 7
- [17] Younghyun Jo and Seon Joo Kim. Practical single-image super-resolution using look-up table. In *2021 IEEE/CVF Conference on Computer Vision and Pattern Recognition (CVPR)*, 2021. 2
- [18] Hakki Can Karaimer and Michael S Brown. A software platform for manipulating the camera imaging pipeline. In *Computer Vision–ECCV 2016: 14th European Conference, Amsterdam, The Netherlands, October 11–14, 2016, Proceedings, Part I 14*, pages 429–444. Springer, 2016. 2
- [19] Hakki Can Karaimer and Michael S Brown. A software platform for manipulating the camera imaging pipeline. In *Computer Vision–ECCV 2016: 14th European Conference, Amsterdam, The Netherlands, October 11–14, 2016, Proceedings, Part I 14*, pages 429–444. Springer, 2016. 2
- [20] Muhammad Murtaza Khan, Jocelyn Chanussot, Laurent Condat, and Annick Montanvert. Indusion: Fu-

- sion of multispectral and panchromatic images using the induction scaling technique. *IEEE Geoscience and Remote Sensing Letters*, 5(1):98–102, 2008. 1, 3
- [21] Craig A Laben and Bernard V Brower. Process for enhancing the spatial resolution of multispectral imagery using pan-sharpening, 2000. US Patent 6,011,875. 4, 7
- [22] Jiacheng Li, Chang Chen, Zhen Cheng, and Zhiwei Xiong. Mlut: Cooperating multiple look-up tables for efficient image super-resolution. In *European conference on computer vision*, pages 238–256. Springer, 2022. 2
- [23] Wenhao Li, Guangyang Wu, Wenyi Wang, Peiran Ren, and Xiaohong Liu. Fastllve: Real-time low-light video enhancement with intensity-aware look-up table. In *Proceedings of the 31st ACM International Conference on Multimedia*, pages 8134–8144, 2023. 2
- [24] Huangxing Lin, Yunlong Lin, Jingyuan Xia, Linyu Fan, Feifei Li, Yingying Wang, and Xinghao Ding. Fusion2void: Unsupervised multi-focus image fusion based on image inpainting. *IEEE Transactions on Circuits and Systems for Video Technology*, 2024. 4
- [25] Yunlong Lin, Zhenqi Fu, Ge Meng, Yingying Wang, Yuhang Dong, Linyu Fan, Hedeng Yu, and Xinghao Ding. Domain-irrelevant feature learning for generalizable pan-sharpening. In *Proceedings of the 31st ACM International Conference on Multimedia*, pages 3287–3296, 2023. 4
- [26] Yunlong Lin, Zhenqi Fu, Kairun Wen, Tian Ye, Sixiang Chen, Ge Meng, Yingying Wang, Yue Huang, Xiaotong Tu, and Xinghao Ding. Unsupervised low-light image enhancement with lookup tables and diffusion priors. *arXiv preprint arXiv:2409.18899*, 2024. 2
- [27] Yunlong Lin, Tian Ye, Sixiang Chen, Zhenqi Fu, Yingying Wang, Wenhao Chai, Zhaohu Xing, Lei Zhu, and Xinghao Ding. Aglldiff: Guiding diffusion models towards unsupervised training-free real-world low-light image enhancement. *arXiv preprint arXiv:2407.14900*, 2024. 2
- [28] Guandu Liu, Yukang Ding, Mading Li, Ming Sun, Xing Wen, and Bin Wang. Reconstructed convolution module based look-up tables for efficient image super-resolution. In *Proceedings of the IEEE/CVF International Conference on Computer Vision*, pages 12217–12226, 2023. 2, 3
- [29] JG Liu. Smoothing filter-based intensity modulation: A spectral preserve image fusion technique for improving spatial details. *International Journal of remote sensing*, 21(18):3461–3472, 2000. 4, 7
- [30] Cheng Ma, Jingyi Zhang, Jie Zhou, and Jiwen Lu. Learning series-parallel lookup tables for efficient image super-resolution. In *European Conference on Computer Vision*, pages 305–321. Springer, 2022. 2, 3
- [31] Jiayi Ma, Wei Yu, Chen Chen, Pengwei Liang, Xiaojie Guo, and Junjun Jiang. Pan-gan: An unsupervised pan-sharpening method for remote sensing image fusion. *Information Fusion*, 62:110–120, 2020. 4, 7
- [32] Giuseppe Masi, Davide Cozzolino, Luisa Verdoliva, and Giuseppe Scarpa. Pansharpening by convolutional neural networks. *Remote Sensing*, 8(7):594, 2016. 2, 3, 4, 7
- [33] Ge Meng, Jingjia Huang, Yingying Wang, Zhenqi Fu, Xinghao Ding, and Yue Huang. Progressive high-frequency reconstruction for pan-sharpening with implicit neural representation. In *Proceedings of the AAAI Conference on Artificial Intelligence*, pages 4189–4197, 2024. 2
- [34] Frosti Palsson, Johannes R Sveinsson, and Magnus O Ulfarsson. A new pansharpening algorithm based on total variation. *IEEE Geoscience and Remote Sensing Letters*, 11(1):318–322, 2013. 1, 3
- [35] Lucien Wald. *Data fusion: definitions and architectures: fusion of images of different spatial resolutions*. Presses des MINES, 2002. 7
- [36] Lucien Wald, Thierry Ranchin, and Marc Mangolini. Fusion of satellite images of different spatial resolutions: Assessing the quality of resulting images. *Photogrammetric engineering and remote sensing*, 63(6):691–699, 1997. 6
- [37] Jiaming Wang, Tao Lu, Xiao Huang, Ruiqian Zhang, and Xiaoxiao Feng. Pan-sharpening via conditional invertible neural network. *Information Fusion*, 101:101980, 2024. 4, 7
- [38] Tao Wang, Yong Li, Jingyang Peng, Yipeng Ma, Xian Wang, Fenglong Song, and Youliang Yan. Real-time image enhancer via learnable spatial-aware 3d lookup tables. In *Proceedings of the IEEE/CVF International Conference on Computer Vision*, pages 2471–2480, 2021. 2
- [39] Yingying Wang, Yunlong Lin, Ge Meng, Zhenqi Fu, Yuhang Dong, Linyu Fan, Hedeng Yu, Xinghao Ding, and Yue Huang. Learning high-frequency feature enhancement and alignment for pan-sharpening. In *Proceedings of the 31st ACM International Conference on Multimedia*, pages 358–367, 2023. 2
- [40] Yingying Wang, Xuanhua He, Yuhang Dong, Yunlong Lin, Yue Huang, and Xinghao Ding. Cross-modality interaction network for pan-sharpening. *IEEE Transactions on Geoscience and Remote Sensing*, 2024. 2
- [41] Yingying Wang, Yunlong Lin, Xuanhua He, Hui Zheng, Keyu Yan, Linyu Fan, Yue Huang, and Xinghao Ding. Learning diffusion high-quality priors for pan-sharpening: A two-stage approach with time-

- aware adapter fine-tuning. *IEEE Transactions on Geoscience and Remote Sensing*, 2025. 3, 4, 7
- [42] Yingying Wang, Hui Zheng, Feifei Li, Yunlong Lin, Linyu Fan, Xuanhua He, Yue Huang, and Xinghao Ding. Towards generalizable pan-sharpening: Conditional flow-based learning guided by implicit high-frequency priors. *IEEE Transactions on Geoscience and Remote Sensing*, 2025. 4
- [43] Zhou Wang, Alan C Bovik, Hamid R Sheikh, and Eero P Simoncelli. Image quality assessment: from error visibility to structural similarity. *IEEE transactions on image processing*, 13(4):600–612, 2004. 7
- [44] Shuang Xu, Jiangshe Zhang, Zixiang Zhao, Kai Sun, Junmin Liu, and Chunxia Zhang. Deep gradient projection networks for pan-sharpening. In *Proceedings of the IEEE/CVF Conference on Computer Vision and Pattern Recognition*, pages 1366–1375, 2021. 3, 4
- [45] Keyu Yan, Man Zhou, Jie Huang, Feng Zhao, Chengjun Xie, Chongyi Li, and Danfeng Hong. Panchromatic and multispectral image fusion via alternating reverse filtering network. *Advances in Neural Information Processing Systems*, 35:21988–22002, 2022. 3
- [46] Keyu Yan, Man Zhou, Li Zhang, and Chengjun Xie. Memory-augmented model-driven network for pan-sharpening. In *European Conference on Computer Vision*, pages 306–322. Springer, 2022. 3
- [47] Keyu Yan, Man Zhou, Li Zhang, and Chengjun Xie. Memory-augmented model-driven network for pan-sharpening. In *European Conference on Computer Vision*, pages 306–322. Springer, 2022. 1
- [48] Gang Yang, Xiangyong Cao, Wenzhe Xiao, Man Zhou, Aiping Liu, Xun Chen, and Deyu Meng. Panflownet: A flow-based deep network for pan-sharpening. In *Proceedings of the IEEE/CVF International Conference on Computer Vision*, pages 16857–16867, 2023. 4, 7
- [49] Junfeng Yang, Xueyang Fu, Yuwen Hu, Yue Huang, Xinghao Ding, and John Paisley. Pannet: A deep network architecture for pan-sharpening. In *Proceedings of the IEEE international conference on computer vision*, pages 5449–5457, 2017. 3
- [50] Qiangqiang Yuan, Yancong Wei, Xiangchao Meng, Huanfeng Shen, and Liangpei Zhang. A multiscale and multidepth convolutional neural network for remote sensing imagery pan-sharpening. *IEEE Journal of Selected Topics in Applied Earth Observations and Remote Sensing*, 11(3):978–989, 2018. 3, 4, 7
- [51] Roberta H Yuhas, Alexander FH Goetz, and Joe W Boardman. Discrimination among semi-arid landscape endmembers using the spectral angle mapper (sam) algorithm. In *JPL, Summaries of the Third Annual JPL Airborne Geoscience Workshop. Volume 1: AVIRIS Workshop*, 1992. 7
- [52] Hui Zeng, Jianrui Cai, Lida Li, Zisheng Cao, and Lei Zhang. Learning image-adaptive 3d lookup tables for high performance photo enhancement in real-time. *IEEE Transactions on Pattern Analysis and Machine Intelligence*, page 1–1, 2020. 2
- [53] Feng Zhang, Kai Zhang, Jiande Sun, Jian Wang, and Lorenzo Bruzzone. Drformer: Learning disentangled representation for pan-sharpening via mutual information-based transformer. *IEEE Transactions on Geoscience and Remote Sensing*, 62:1–15, 2023. 2, 4
- [54] Jie Zhang, Ke Cao, Keyu Yan, Yunlong Lin, Xuanhua He, Yingying Wang, Rui Li, Chengjun Xie, Jun Zhang, and Man Zhou. Frequency decoupled domain-irrelevant feature learning for pan-sharpening. *IEEE Transactions on Circuits and Systems for Video Technology*, 2024. 4
- [55] Kaiwen Zheng, Jie Huang, Man Zhou, Danfeng Hong, and Feng Zhao. Deep adaptive pansharpening via uncertainty-aware image fusion. *IEEE Transactions on Geoscience and Remote Sensing*, 61:1–15, 2023. 1
- [56] Yu Zhong, Xiao Wu, Liang-Jian Deng, Zihan Cao, and Hong-Xia Dou. Ssdif: Spatial-spectral integrated diffusion model for remote sensing pansharpening. *Advances in Neural Information Processing Systems*, 37: 77962–77986, 2025. 2
- [57] Huanyu Zhou, Qingjie Liu, and Yunhong Wang. Panformer: A transformer based model for pan-sharpening. In *2022 IEEE International Conference on Multimedia and Expo (ICME)*, pages 1–6. IEEE, 2022. 2, 4
- [58] Huanyu Zhou, Qingjie Liu, Dawei Weng, and Yunhong Wang. Unsupervised cycle-consistent generative adversarial networks for pan sharpening. *IEEE Transactions on Geoscience and Remote Sensing*, 60:1–14, 2022. 4, 7
- [59] Man Zhou, Jie Huang, Yanchi Fang, Xueyang Fu, and Aiping Liu. Pan-sharpening with customized transformer and invertible neural network. In *Proceedings of the AAAI conference on artificial intelligence*, pages 3553–3561, 2022. 2, 4
- [60] Man Zhou, Jie Huang, Keyu Yan, Hu Yu, Xueyang Fu, Aiping Liu, Xian Wei, and Feng Zhao. Spatial-frequency domain information integration for pan-sharpening. In *European conference on computer vision*, pages 274–291. Springer, 2022. 4, 7
- [61] Man Zhou, Keyu Yan, Xueyang Fu, Aiping Liu, and Chengjun Xie. Pan-guided band-aware multi-spectral feature enhancement for pan-sharpening. *IEEE Transactions on Computational Imaging*, 9:238–249, 2023. 1

- [62] Zeyu Zhu, Xiangyong Cao, Man Zhou, Junhao Huang, and Deyu Meng. Probability-based global cross-modal upsampling for pansharpening. In *Proceedings of the IEEE/CVF Conference on Computer Vision and Pattern Recognition*, pages 14039–14048, 2023. [3](#)